JOURNAL OF PROPULSION AND POWER
Vol. 25, No. 3, May–June 2009

Design of a Quiet Propeller for an Electric Mini Unmanned Air Vehicle

Ohad Gur* and Aviv Rosen†
Technion—Israel Institute of Technology, Haifa 32000, Israel

DOI: 10.2514/1.38814

Designing a quiet and efficient propeller is a demanding task because these two goals often lead to contradictory design trends. The task becomes even more complicated when additional constraints are introduced. This paper presents a multidisciplinary design optimization process for designing a quiet propeller under various constraints. The acoustic model of the propeller is presented in detail, including its validation. The new process is used to design a quiet propeller for an electric mini unmanned air vehicle. This design is subjected to power, structural, and side constraints. The design variables include blade geometry, blade cone angle, propeller radius, number of blades, and rotational speed. It is shown that the motor characteristics have an important influence on the optimization, and it is therefore important to take them into account during the design process. The influences of the various parameters on the design and propeller's characteristics are presented and discussed in detail.

Nomenclature

a	=	speed of sound
C_L, C_D	=	vehicle's lift and drag coefficients
C_{li}	=	cross-sectional design lift coefficient
c	=	chord
dS	=	surface element of a noise source
F_i	=	component of the aerodynamic force that acts on the noise source
f	=	function
f	=	noise frequency
i, j, k	=	indices
I_{in}	=	driver's input current
K_V	=	motor's speed constant equal to the inverse of the back-electromotive-force constant
M	=	Mach number
$\mathbf{M}$	=	Mach number vector
M_r	=	projection of $\mathbf{M}$ onto $\mathbf{r}_{\text{rel}}$
N_b	=	number of blades
P_B	=	power extracted from the battery
P_P	=	propeller's required power (equal to motor's output power)
p_{AFFTi}	=	ith harmonic of an A-weighted pressure wave
$p_{\text{FFT}i}$	=	ith harmonic of a pressure wave
p_{ref}	=	reference pressure
$\bar{p}^2$	=	mean square average of sound pressure
$\bar{p}_A^2$	=	mean square average of sound pressure (A-weighted)
R	=	propeller's radius
R_a	=	motor resistance
r	=	radial/spanwise coordinate
$\mathbf{r}_{\text{rel}}$	=	position vector of an observer relative to the noise source
r_{rel}	=	magnitude of $\mathbf{r}_{\text{rel}}$
$\hat{\mathbf{r}}_{\text{rel}}$	=	unit vector in the direction of $\mathbf{r}_{\text{rel}}$
SPL	=	sound pressure level
$\text{SPL}_{\text{harmonic } i}$	=	ith harmonic of a sound pressure level
SPLA	=	A-weighted sound pressure level
$\text{SPLA}_{\text{harmonic } i}$	=	ith harmonic of an A-weighted sound pressure level
T	=	thrust
$\mathbf{T}$	=	Lighthill stress tensor
t	=	time
th	=	thickness
t_C	=	time duration of a noise cycle
t_l	=	loitering time
V_{in}	=	driver's input voltage
V_F	=	flight velocity
$\mathbf{v}$	=	velocity vector of a noise source
$\mathbf{x}$	=	position vector of a noise source
β	=	pitch angle
γ	=	cone angle
$\Delta_{\text{dBA}-\text{dB}}$	=	difference between $\text{SPL}_{\text{harmonic } i}$ and $\text{SPLA}_{\text{harmonic } i}$
Δp	=	perturbation of static pressure
$\Delta \mathbf{p}_{ij}$	=	generalized stress tensor
Δp_{thick}, $\Delta p_{\text{loading}}$	=	thickness and loading noise pressure perturbations
δ	=	Kronecker's delta function
η_S	=	motor system's efficiency
η_D	=	driver's efficiency
ρ_a	=	air density
$\bar{\sigma}$	=	von Mises stress
τ	=	retarded time
Ψ_0	=	volume of a noise source
Ω	=	propeller's rotational speed

Presented as Paper 3073 at the 14th AIAA/CEAS Aeroacoustics Conference, Vancouver, Canada, 5–7 May 2008; received 29 May 2008; revision received 4 June 2008; accepted for publication 27 January 2009.

*Researcher, Faculty of Aerospace Engineering; ohadg@aerodyne.technion.ac.il. Member AIAA.

†Professor, Faculty of Aerospace Engineering; rosen@aerodyne.technion.ac.il. Fellow AIAA.

I. Introduction

TODAY, renewed attention is being focused on the first aeronautical propulsion device: the propeller. This is due to the increased use of unmanned air vehicles (UAVs) [1,2], the growing market of general aviation [2], the increasing interest in ultralight categories or light sport air vehicles, and the growing importance of environmental issues that have led to the development of all-electric emissionless aircraft [2,3].

One of the most disturbing problems of propeller-driven aircraft is their noise, which may limit the aircraft's operation. Many airports around the world impose strict limitations on noise level permitted during day or night. The acoustic signature of military aircraft has a significant effect on their detection. The importance of the noise signature of propeller-driven air vehicles was already noticed during

the 1960s [4] and led to the development of the YO-3A Quiet Star that later became an acoustic research aircraft [5]. Today, with the increased use of propeller-driven UAVs, there is a renewed interest in reducing the noise of propellers [6].

In propeller-based propulsion systems, the main sources of noise are the engine and the propeller. Reducing the engine noise can be achieved by developing a suitable exhaust pipe or by using electric motors. Many of today's mini unmanned aerial vehicle's use electric motors [7–10].

Reducing the propeller's noise requires special attention during its design. Noise reduction can be achieved by a systematic design of the propeller's geometry and aerodynamic characteristics. Yet, these same characteristics determine the performance and efficiency of the entire propulsion system. In many cases, efficiency and noise reduction result in contradictory design trends. This makes the design of an efficient and quiet propeller a task that requires a multidisciplinary design optimization (MDO) approach [11].

In many cases, the propeller is the simplest and most inexpensive element of a propeller-based propulsion system, yet its design has an enormous influence on the efficiency and noise level of the entire vehicle. Furthermore, in many cases, the configuration of the propulsion system is determined at an early stage of the design, except for the propeller, which can be improved quite easily at later stages of the project or even during operation. Thus, the propeller design is an important element in the process of developing a new quiet air vehicle or reducing the noise of an existing one.

Most of the traditional methods for propeller design are based on the well-known work of Betz [12] from 1919. An example of applying this method is presented in [13]. This approach is based on optimizing the propeller's geometry at a certain specific operating condition (a certain combination of airspeed, altitude, and propeller rotational speed), such that the power that is required to obtain a certain propulsive force at these operating conditions is minimized (or the thrust produced by a certain power is maximized). An example of such a design is the propeller of Rutan's Voyager (the first nonstop, nonrefueled flight around the world) [14].

Betz's method considers only the aerodynamic efficiency of the propeller. It does not consider the propeller noise signature. Thus, for designing a quiet propeller when using Betz's method, a serial design process is used. First, the optimal aerodynamic propeller, with a maximum efficiency, is defined. Then this propeller is modified to reduce its acoustic signature. Such a process has been used extensively for designing quiet propellers [15,16]. The main problem of such an iterative process is that it does not ensure that the final design will be optimal. It is also difficult to introduce additional constraints into this serial design process, such as side or structural constraints.

As already mentioned, the best approach for solving such a design problem is to use MDO. MDO ensures that all the different disciplines are addressed simultaneously. Thus, the best compromise between contradictory goals of an efficient and a quite propeller will be reached. This kind of approach has been already applied to propeller designs. Ormsbee and Woan [17] presented an optimization procedure of the circulation distribution along a propeller's blades to minimize noise signature under performance constraints using simplified models. Succi [15] and Miller and Sullivan [18] showed several ways to decrease a propeller's noise while maintaining its efficiency. Burger et al. [19] used a vortex lattice approach and genetic algorithm to design an efficient and quiet propeller. Most of the past investigations did not consider the characteristics of the power plant itself (the motor). This may have a significant effect on the efficiency of the entire propulsion system and thus on the optimal propeller design. References [20–22] present examples of propeller designs for specific vehicles, which represent a compromise between aerodynamic and acoustic constraints. Most of the previous investigations used a very limited number of design variables rather than the full range of the parameters that are under the authority of the designer. The design methods already presented considered the influence of the noise level on the propeller efficiency with minor (and sometimes no) consideration of the structural integrity of the blades.

The paper will present a process for designing a quiet propeller while taking into account performance and structural constraints. It will be shown that the motor characteristics play an important role in the design. First, the analysis tools (including aerodynamic, structural, and acoustic models) will be described. Because noise is the subject matter of the present paper, the acoustic model will be described in more detail and its validation will be discussed. Then the optimization procedure and design process will be presented. The application of the method for designing a quiet propeller for an electric UAV will be presented in detail. The influence on the optimal design of performance constraints, structural constraints, and number of blades will be shown and discussed.

II. Analysis Tools

Analysis tools for propeller design include an aerodynamic model, a structural model, and an acoustic model. The selection of the appropriate model is based on the following two considerations:

1) It should be sufficiently accurate.

2) It should be efficient, because the optimization procedure includes a very high number of iterations.

The aerodynamic model calculates the distribution of the aerodynamic loads along the propeller blades. This data is used to calculate the propeller's thrust and required power. In addition, the distribution of the aerodynamic loads is used as an input for the structural and acoustic analyses. Consequently, an inaccurate aerodynamic model may result in inaccuracies in the other analyses of the propeller. In the present case, a momentum/blade-element model is used.

For regular design conditions of propellers (axial uniform flow and high advance ratios), the blade's cross sections do not experience stall and the momentum/blade-element model gives results of high accuracy [23]. The blade-element/momentum analysis can be extended to include the influence of rotation on the aerodynamic behavior of cross sections after reaching stall [24]. Momentum/blade-element models are usually much more efficient than other models, and thus they are suitable for the present MDO analysis.

A structural analysis is essential to ensure that the propeller blades will be able to withstand the aerodynamic and inertial loads that act along them. Common tools for the structural analysis of blades are finite element models [25]. Yet, finite element models require relatively large computer resources and computing time. Thus, a more efficient rod model using a transfer-matrix formulation will be applied [26].

The rod structural model describes the propeller blades as a series of straight segments located along the blade's elastic axis, which is not necessarily a straight line. The structural cross-sectional properties are uniform along each segment and equal to the structural properties of a representative cross section of that segment. The transfer-matrix problem is solved using the boundary conditions of a cantilevered rod (clamped root and free tip). The solution procedure is very efficient and the results are very accurate [26].

III. Acoustic Model

A. Noise Equations

Most of the models used to calculate a propeller's noise signature are based on a solution of the constrained wave equation, known as the Ffowcs-Williams/Hawkings equation [27]:

$$\frac{1}{a^2}\cdot\frac{\partial^2(\Delta p)}{\partial t^2}-\frac{\partial^2(\Delta p)}{\partial x_i^2}=\frac{\partial^2 T_{ij}}{\partial x_i\cdot\partial x_j}+\frac{\partial}{\partial t}\left\{\rho_a\cdot v_i\cdot\delta(f)\cdot\frac{\partial f}{\partial x_i}\right\}-\nabla\left\{\Delta p_{ij}\cdot\delta(f)\cdot\frac{\partial_f}{\partial x_j}\right\} \tag{1}$$

where a is the speed of sound, Δp is the perturbation in the static pressure (relative to the undisturbed pressure), t is the observer time, and $\mathbf{x}$ is the position vector of the noise source relative to a stationary system of coordinates (with components x_i). $\mathbf{T}$ is Lighthill stress tensor (with components T_{ij}), $\Delta\mathbf{p}$ is the generalized stress tensor

(with components Δp_{ij}), $\mathbf{v}$ is the source velocity vector (with components v_i), δ is Kronecker's delta function, and f is a function that defines the surface of the body producing the pressure wave (in the present case, it defines the surfaces of the blades):

$$f(\mathbf{x}) = \begin{cases} <0 & \mathbf{x} \text{ inside the body} \\ 0 & \mathbf{x} \text{ on the body surface} \\ >0 & \mathbf{x} \text{ outside the body} \end{cases} \tag{2}$$

There are three forcing terms on the right-hand side of Eq. (1): vortex, thickness, and loading terms (from left to right) [28]. It was shown that for thin blades with cross sections operating in subsonic or transonic conditions, the vortex term can be neglected [29]. Thus, the solution of the Ffowcs-Williams/Hawkings equation includes two terms: the thickness noise Δp_{thick} and the loading noise $\Delta p_{\text{loading}}$:

$$\Delta p(\mathbf{x}, t) = \Delta p_{\text{thick}}(\mathbf{x}, t) + \Delta p_{\text{loading}}(\mathbf{x}, t) \tag{3}$$

The solution of the Ffowcs-Williams/Hawkings equation is obtained after applying Green's function [27]. This solution is then discretized [30] and the following approximations are adopted:

1) The velocity of the noise source is subsonic.

2) The noise source is much faster than the observer.

3) The propeller's rotational speed and the velocity of the air vehicle do not vary with time.

The final expressions for the loading and thickness noise become [15]

$$\Delta p_{\text{loading}}(\mathbf{x}, t) = \frac{1}{4 \cdot \pi} \sum_k \Bigg\{ \underbrace{\frac{\dot{\mathbf{F}} \cdot \hat{\mathbf{r}}_{\text{rel}} + \mathbf{F} \cdot \hat{\mathbf{r}}_{\text{rel}} \cdot [(\dot{\mathbf{M}} \cdot \hat{\mathbf{r}}_{\text{rel}})/(1 - M_r)]}{r_{\text{rel}} \cdot a \cdot (1 - M_r)^2}}_{\text{far field}} + \underbrace{\frac{\mathbf{F} \cdot \hat{\mathbf{r}}_{\text{rel}} \cdot [(1 - \mathbf{M} \cdot \mathbf{M})/(1 - M_r)] - \mathbf{F} \cdot \mathbf{M}}{r_{\text{rel}}^2 \cdot (1 - M_r)^2}}_{\text{near field}} \Bigg\}_k \tag{4}$$

$$\Delta p_{\text{thick}}(\tilde{\mathbf{x}}, t) = \frac{\rho}{4.\pi} \sum_k \left\{ \frac{\Psi_0}{r_{\text{rel}} \cdot (1 - M_r)^3} \cdot \left[\frac{\ddot{M}_r}{1 - M_r} + 3 \left(\frac{\dot{M}_r}{1 - M_r} \right)^2 + \frac{\dot{M}_r \cdot a \cdot (1 + 2 \cdot M_r)}{r_{\text{rel}} \cdot (1 - M_r)} + 2 \left(\frac{M_r \cdot a}{r_{\text{rel}}} \right)^2 \right] \right\}_k \tag{5}$$

where Σ indicates integration over the entire body that generates noise, $\mathbf{r}_{\text{rel}}$ is the location vector of the observer relative to the noise source, r_{rel} is the magnitude of $\mathbf{r}_{\text{rel}}$, $\hat{\mathbf{r}}_{\text{rel}}$ is a unit vector in the direction of $\mathbf{r}_{\text{rel}}$, $\mathbf{M}$ is the Mach vector, defined as

$$\mathbf{M} = \frac{\mathbf{v}}{a} \tag{6}$$

M_r is the projection of $\mathbf{M}$ onto $\mathbf{r}_{\text{rel}}$, $\mathbf{F}$ is the aerodynamic loading force acting on the element, and Ψ_0 is the volume of the blade element.

A dot accent indicates a time derivative at the noise source system (differentiation relative to the retarded time). If t is the time as measured in the observer's frame of reference, the retarded time τ indicates the time when the pressure wave left the noise source:

$$\tau = t - \frac{r_{\text{rel}}(\tau)}{a} \tag{7}$$

The loading noise [Eq. (4)] is composed of two components: the far-field and near-field loading noise. These two terms differ by the power of r_{rel} in the denominator. The far-field term is proportional to $1/r_{\text{rel}}$, the near-field term is proportional to $1/r_{\text{rel}}^2$, and thus the last term becomes relatively small at large distances from the noise source.

Calculations of the noise produced by a propeller are based on dividing the propeller's blades into small elements (similar to the aerodynamic blade elements). The pressure at a certain point in space at a certain time is obtained by summing up the contributions of all the elements according to Eqs. (4) and (5). Then the same process is repeated for the next time step, in which the new positions of the air vehicle and propeller blades at that time are considered. The pressure wave is defined after repeating this process for a complete cycle (e.g., for a two-bladed propeller, one noise cycle is equivalent to half of a revolution).

B. Spectral Analysis

If the pressure wave Δp is known, its spectral analysis defines the sound pressure level (SPL) and its different harmonics. The mean square average of the sound pressure, $\bar{p}^2$, and the resultant SPL (given in decibels) are defined as follows:

$$\bar{p}^{\,2} = \frac{1}{t_C} \int_0^{t_C} \Delta p^2(\mathbf{x}, t) \tag{8}$$

$$\text{SPL dB} = 10 \cdot \log_{10} \frac{\bar{p}^2}{p_{\text{ref}}^2} \tag{9}$$

where t_C is the time duration of a noise cycle. The reference pressure for air is usually chosen as $p_{\text{ref}} = 20 \times 10^{-6}$ Pa.

Using fast Fourier transform (FFT), the different harmonics of the pressure wave $p_{\text{FFT}i}$ and the sound pressure harmonics $\text{SPL}_{\text{harmonic } i}$ are calculated:

$$\bar{p}^{\,2} = \sum_i \frac{1}{2} \cdot p_{\text{FFT}i}^2 \tag{10}$$

$$\text{SPL}_{\text{harmonic } i} \text{ dB} = 10 \cdot \log_{10} \left(\frac{p_{\text{FFT}i}}{p_{\text{ref}}} \right)^2 \tag{11}$$

The noise sensitivity of the human ear depends on the noise frequency f. It is common to define sound harmonics representing the human ear sensitivity through the A-weighted sound pressure level $\text{SPLA}_{\text{harmonic } i}$. The differences between $\text{SPL}_{\text{harmonic } i}$ and $\text{SPLA}_{\text{harmonic } i}$ are given by the empirical function $\Delta_{\text{dBA-dB}}(\text{f})$ [31]:

$$\text{SPLA}_{\text{harmonic } i} = \text{SPL}_{\text{harmonic } i} + \Delta_{\text{dBA-dB}}(\text{f}) \tag{12}$$

Similar to Eqs. (10) and (11), the following terms are defined:

$$\text{SPLA dBA} = 10 \cdot \log_{10} \left[\frac{\bar{p}_A^2}{p_{\text{ref}}^2} \right] = 10 \cdot \log_{10} \left[\sum_i \frac{1}{2} \cdot p_{A\text{FFT}i}^2 \right] + 10 \cdot \log_{10} \left(\frac{1}{p_{\text{ref}}^2} \right) \tag{13}$$

$$\text{SPLA}_{\text{harmonic } i} \text{ dB} = 10 \cdot \log_{10} \left(\frac{p_{A\text{FFT}i}}{p_{\text{ref}}} \right)^2 \tag{14}$$

Substitution of Eq. (14) into Eq. (13) results in

$$\text{SPLA dBA} = 10 \cdot \log_{10} \left[\sum_i \frac{1}{2} \cdot 10^{\left[\text{SPLA}_{\text{harmonic } i} - 10 \cdot \log_{10} \left(\frac{1}{p_{\text{ref}}^2} \right) \right] / 10} \right] + 10 \cdot \log_{10} \left(\frac{1}{p_{\text{ref}}^2} \right) \tag{15}$$

C. Model Validation

The model validation includes comparisons of the model results with wind-tunnel [32] and flight-test [33] results. The wind-tunnel test included a two-bladed propeller of radius $R = 1.015$ m. The pressure wave and the sound pressure level were measured at different locations relative to the propeller.

Table 1 SPL (in decibels) as obtained by calculations and measured in the wind tunnel [32]

Run BC-61		Run BC-2		Run AC-1		
Calculations	Test	Calculations	Test	Calculations	Test	Microphone location
116.6	119.5	103.3	102.5	102.3	101.1	1
131.2	129.6	111.8	109.1	110.3	108.1	4
129.7	128.6	110.4	108.7	108.9	105.9	9

Table 1 presents a comparison of SPL for three runs (designated as BC-61, BC-2, and AC-1) and three microphone locations (1, 4, and 9). The exact definitions of the test conditions and microphone locations are given in [32]. Comparisons between calculated and measured results exhibit good agreement. The maximum difference does not exceed 1–2 dB. Figures 1 and 2 present two examples of the pressure wave and harmonics.

The flight tests reported in [33] included a Twin Otter aircraft equipped with two microphones (fore and aft). The aircraft has two three-bladed propellers. Four representative flight conditions (designated as cases 1–4) are considered, which are defined in [34].

Table 2 presents a comparison between SPL calculations and flight-test measurements. The differences at the fore microphone are 1–2 dB, and at the aft microphone, the differences reach 5 dB. The higher differences in the aft microphone are probably due to wake influences.

Figures 3 and 4 present the SPL harmonics for two cases (1 and 4). Similar to the results presented in Table 2, the comparison between the fore microphone results and model calculations exhibits good agreement, whereas in the case of the aft microphone, the agreement deteriorates.

IV. Optimal Design of a Quiet Propeller

Any optimal design problem can be described mathematically as a search process for a design configuration that minimizes (or maximizes) a specific cost function that represents the design goal. This search process is usually carried out under certain design constraints.

Any design process requires an a priori definition of design variables, design constraints, and cost function. The design variables are parameters that are determined by the designer. In the general case of a propeller design, these variables are divided into three categories: general design variables, blade design variables, and cross-sectional design variables. The general design variables affect the global configuration of the propeller system and may include the following parameters: number of propellers, number of blades N_b, propeller radius R, and rotational speed Ω. The blade design variables are parameters defining the geometry and structure of each blade [namely, the distribution along the blade of the following parameters: pitch angle $\beta(r)$, chord $c(r)$, sweep angle, dihedral angle (cone angle in the simplest case), mass and inertia, and structural properties].

The blade's cross-sectional design variables define the cross-sectional airfoil geometry as a function of a chordwise coordinate. In the following examples, the cross sections will belong to the NACA-16 airfoil family [35]; thus, the geometry of each cross section is defined by two parameters that vary along the blade: thickness ratio $\mathrm{th}/c(r)$ and design lift coefficient $C_{li}(r)$.

The design constraints may include any kind of constraint: for example, minimum or maximum chord size, allowable maximum stress, etc.

The cost function is a quantitative measure of achieving the design goal: namely, the cost function presents a measure of the quality of the design.

A penalty method is used to solve the constrained optimization problem [36]. A new constrained cost function is defined and minimized to find the optimal design, subject to the constraints.

A. Optimization Scheme

The optimization scheme used here includes a mixed-strategy approach combining three different optimization methods:

1) A heuristic search uses a simple genetic algorithm (SGA) [37].

2) An enumerative scheme uses Nelder and Mead's [38] simplex scheme.

3) A derivative-based scheme uses the steepest-descent method [36].

The SGA [37] simulates a natural selection process, similar to an evolution process. It includes three major elements: reproduction, crossover, and mutation. Starting from an initial random population of designs and using a genetic scheme leads to an improved population.

The next stage of the optimization scheme includes an enumerative simplex scheme [38]. This scheme is capable of dealing efficiently with a large number of design variables, including smoothing constraints of the distributions of variables along the blade.

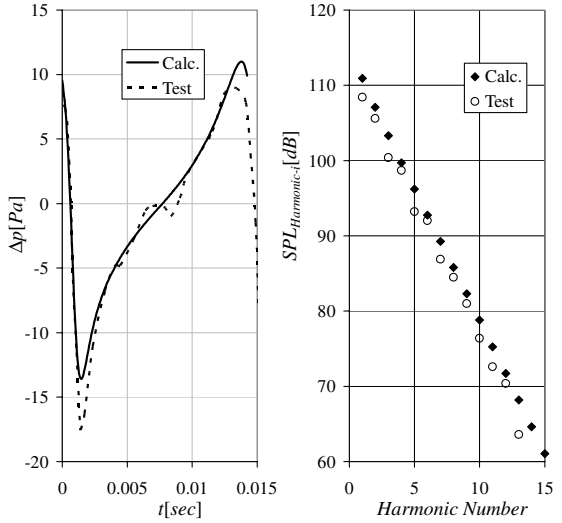

Fig. 1 Comparison between calculations and wind-tunnel results [32] for run AC-1 and microphone 4.

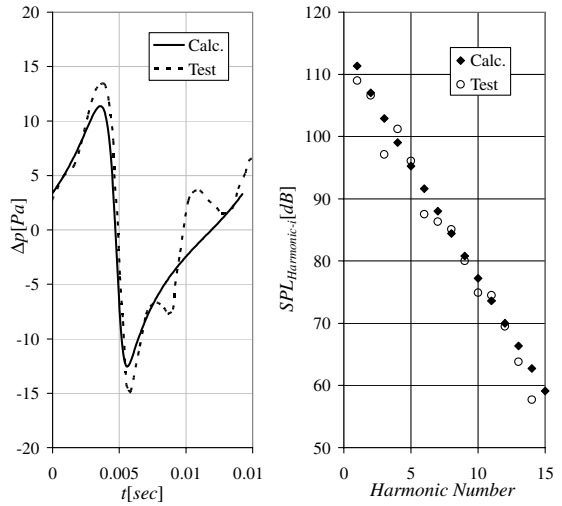

Fig. 2 Comparison between calculations and wind-tunnel results [32] for run BC-2 and microphone 9.

Table 2 SPL (in decibels) as obtained by calculations and measured during flight tests [33]

	Case 4		Case 3		Case 2		Case 1	
	Fore	Aft	Fore	Aft	Fore	Aft	Fore	Aft
Test	113.6	115.9	106.5	112.4	106.7	108.3	115.4	119.3
Calculations	113.4	111.0	107.6	107.2	104.9	105.0	115.2	114.1

A derivative-based method is used only during the final stage of the entire search, to pinpoint the final design. Derivative-based methods are extensively used [36] and are very efficient in unimodal cases (in which the cost function has only one minimum) or in the neighborhood of the global minimum.

The use of a mixed-scheme strategy for optimization (starting with SGA, then using the simplex method, and, finally, applying the steepest-descent method) exploits the various advantages of each scheme [39], as indicated by Table 3. It ensures a thorough search for the global minimum. A detailed description of this strategy and an example of its use are presented in [40].

B. Design Process

The first stage of the design process includes definitions of the cost function (design goal), design variables, and constraints. In cases of complex problems, it is often recommended to start with a simpler problem that includes a simpler cost function and a reduced number of design variables or constraints. This simpler problem helps to better understand the actual problem and to investigate the optimal design trends. It can also be used as an initial design point for the more complex problem.

The design usually starts with a SGA. This scheme does not depend on a specific initial design and is capable of searching through a very wide range of designs to find the global minimum. One of the weaknesses of this scheme is the serrated nature of the distributions of the various design variables along the blade. These distributions are often impractical and should be smoothed. Smoothing can be imposed as a constraint on the absolute magnitude of the second derivative of the variable with respect to the spanwise coordinate. Yet, the SGA scheme becomes inefficient as the number of constraints is increased. Thus, smoothing constraints are usually added only during the second stage of the optimization, which includes the simplex scheme. The smoothing constraints should be imposed in a gradual manner; otherwise, difficulties in convergence are encountered.

At the end of the simplex scheme's application, the design is usually very close to its final form. In most cases, the steepest-descent scheme results in only small changes of the cost function and its effect is mainly to imply final smoothing.

Note that the design process should not be treated as a black box and is by no means fully automatic. The designer plays a major role in the entire process. He or she decides when to switch from one scheme to the other. He or she should follow the results during the application of each scheme and should determine the next steps based on these results. In certain cases, the designer may decide to return to a previous scheme (e.g., when it seems that the solution has converged to a local extremum) or to ease certain constraints to increase the flexibility of the search process and thus examine a wider range of options.

The next section will present the process of designing an optimal propeller for an electric UAV.

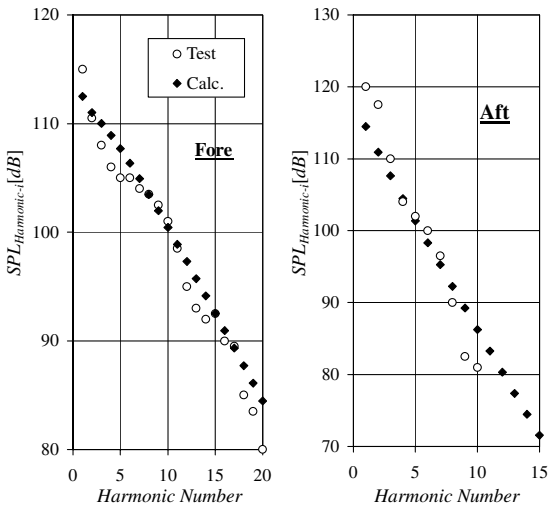

Fig. 3 Comparison between calculations and flight-test results [33] for case 1.

V. Design of a Quiet Propeller for an Electric Mini UAV

An electric mini UAV is considered. The total mass of the vehicle is 5.5 kg. The wing area is 0.72 m^2, and the drag polar of the vehicle is

$$C_D = 0.03 + 0.033 \cdot C_L^2 \tag{16}$$

where C_L and C_D are the vehicle's lift and drag coefficients, respectively.

A direct drive is used (the system does not include a gear box); namely, the rotational speed of the electric motor is equal to that of the propeller, Ω. The parameters that define the characteristics of the electric motor are [8] 1) motor speed constant $K_V = 0.0045$ V · s/rad,[‡] 2) motor resistance $R_a = 0.1$ [Ω], and 3) driver's efficiency $\eta_D = 0.9$.

The electric system's efficiency η_S is defined as the ratio between the propeller's required power P_P and the power that is extracted from the battery, P_B:

$$\eta_s = \frac{P_P}{P_B} \tag{17}$$

where η_S is a function of the input voltage V_{in}, input current I_{in}, and electric driver efficiency η_D:

$$\eta_s = \eta_D \cdot \frac{P_P}{V_{\text{in}} \cdot I_{\text{in}}} \tag{18}$$

For a certain rotational speed Ω and power P_P, V_{in} and I_{in} are calculated by the following equations [8]:

$$V_{\text{in}} = \Omega \cdot K_V + \frac{P_P \cdot R_a}{\Omega \cdot k_V} \tag{19}$$

$$I_{\text{in}} = \frac{P_P}{\Omega \cdot K_V} \tag{20}$$

The main task of the UAV is to loiter at low altitude above a certain area; thus, the goal is to design an optimal propeller for loitering at a speed $V_F = 10$ m/s at sea level. The required thrust under this flight condition, based on the preceding data, is

$$T = 3.5 \text{ N} \tag{21}$$

Because of geometric constraints, the radius of the propeller is limited:

[‡]It is also common to define instead the torque constant (also known as the back-electromotive-force constant), which is the inverse of K_V.

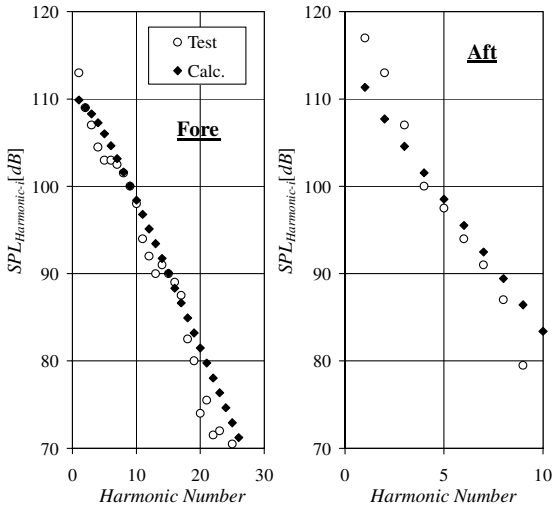

Fig. 4 Comparison between calculations and flight-test results [33] for case 4.

$$R \leq 0.15 \text{ m} \tag{22}$$

NACA-16 cross sections are used. The database for this airfoil family is limited to the following range of thickness ratio th/c and design lift coefficient C_{li} [35]:

$$0.04 < \frac{\tilde{t}}{c} < 0.21 \tag{23}$$

$$0.0 < C_{li} < 0.7 \tag{24}$$

For practical reasons, the chord is also limited:

$$c < 0.052 \text{ m} \tag{25}$$

The design variables of the current design problem are the propeller's radius R; distribution of chord along the blade, $c(r)$; distribution of pitch angle along the blade, $\beta(r)$; distribution of thickness ratio along the blade, th/$c(r)$; and distribution of design lift coefficient along the blade, $C_{li}(r)$.

The distribution of the various parameters is defined by their values at 17 stations along the blade; thus, there are 69 design variables. At a later stage of this study, another design variable will be added: the cone angle of the blades. The energy source of the UAV is a lithium polymer battery with a mass of 2 kg and a capacity of 250 W · h. From this capacity, 150 W · h are allocated for loitering.

The goal of the propeller design is twofold: 1) maximize the loitering time and 2) minimize the noise produced by the UAV. As will be shown in what follows, these are contradictory goals.

To understand the design trends and the physical phenomena behind them, the design will be carried out in a gradual manner. Initially, two-bladed propellers will be considered and the number of design constraints will be increased gradually to understand their influence on the optimal design. Then the influence of the number of blades on the optimal designs will be investigated. Although complex configurations of the blades may offer certain advantages [41], the present study is confined to straight blades.

A. Two-Bladed Propeller

As a first step in studying the problem, two different propellers will be designed for the following two extreme goals:

1) For maximum loitering time, maximize the loitering time t_l subject to the constraints of Eqs. (21–25), without considering any other goals or constraints. The cost function to be minimized is the power extracted from the vehicle's battery, P_B.

2) To minimum noise at loitering, minimize the noise of the vehicle as heard by an observer located 50 m beneath the UAV, subject to the constraints of Eqs. (21–25), without considering any other goals or constraints. The cost function is the SPLA produced by the propeller at the observer point.

The preceding described optimization process has been applied for the design of these two propellers and the results are presented in Table 4 and Fig. 5.

Figure 5 presents the geometry of the optimized propellers: namely, spanwise distributions of the pitch angle β, chord c, and cross-sectional thickness th. The design lift coefficient C_{li} is equal (in both cases) to its upper limit value $C_{li} = 0.7$.

The propeller for maximum loitering time (case 1) operates at a relatively high rotational speed ($\Omega = 13,590$ rpm) and extracts from the battery an electrical power of $P_B = 54$ W, which means a loitering time of $t = 160$ min. Its noise intensity is SPLA= 36.0 dBA.

The propeller for minimum noise (case 2) operates at a much lower rotational speed ($\Omega = 2233$ rpm) and results in a noise intensity of only SPLA = 18.4 dBA, which means a significant noise reduction of 17.6 dBA. This reduction in noise comes at a cost of a significant reduction in the efficiency of the entire propulsion system. This results in an increase in the power extracted from the battery during loitering ($P_B = 357$ W), leading to a loitering time of only $t_l = 25$ min. The significant reduction in the loitering time is due to the increase in the required power by the propeller (from 46 to 54 W) and a significant decrease in the efficiency of the electric motor (from 0.81 in case 1 to 0.15 in case 2).

In both designs, the propeller gives a thrust of $T = 3.5$ N. Because of the very large decrease in the rotational speed, in the case of the propeller for minimum noise, there is a significant increase in the pitch angle and chord length (see Fig. 5). In fact, case 2 is impractical and does not represent a feasible design, because the chord length reaches its limit [Eq. (25)]. Even if design 2 were practical, the loitering time is too short. Thus, to offer a reasonable loitering time, a constraint of the magnitude P_B will be imposed in the next subsection.

B. Two-Bladed Propeller Under Power Constraints

In this case, the cost function remains the SPLA. In addition to the previous constraints, the power that is extracted from the battery, P_B, is limited. Three different cases are considered: $P_B \leq 65, 70, 75$ W.

In Table 4, a summary of the design results is presented. As the allowable P_B increases, the noise decreases, but the loitering time decreases as well. The decrease in the noise is mainly a result of the decrease in the rotational speed, Ω. Unfortunately, this also results in a decrease in the electric motor efficiency and a reduction of the loitering time.

The geometry of the propellers is presented in Fig. 6, together with the geometry of the minimum SPLA propeller of Fig. 5. Because all of the propellers have to produce identical thrust, the decrease in the rotational speed is accompanied by an increase in the pitch angle and chord length along the blade. The increase in chord length also leads to an increase in the thickness of the cross section.

C. Two-Bladed Propeller Under Power and Stress Constraints

From Fig. 6, it is clear that the blades are very thin, and thus they may develop high stresses that will endanger their integrity. Therefore, structural constraints are added in what follows. It is assumed that the blade is made of aluminum 7075-T6. The yield stress of this material is 5.03×10^8 Pa. The maximum von Mises stress $\bar{\sigma}$ will be limited to

$$\bar{\sigma} < 1.5 \times 10^8 \text{ Pa} \tag{26}$$

In the current example, the stresses are calculated during loitering. If necessary (see [40]), it is possible to calculate the stresses under other critical flight conditions such as takeoff or maximum speed.

The influences of the stress constraints on the characteristics of the propeller are presented in Table 4 (denoted as "with stress constraints"). The SPLA increases by 2.9, 1.0, and 0.6 dBA for the cases $P_B \leq 65, 70, 75$ W, respectively, as a result of introducing the

Table 3 Advantages and disadvantages of the various numerical optimization schemes

	Heuristic scheme	Enumerative scheme	Gradient-based scheme
Capability of finding the global optimum	Good	Limited ability	Poor
Pinpointing the local optimum	Poor	Limited ability	Good
Reaching the feasible region subject to a high number of constraints	Poor	Good	Good
Number of iterations needed for convergence	High	High	Low
Required computer resources	High	Low	Relatively low

Table 4 Optimal two-bladed propellers under various design goals and constraints

Design description	SPLA, min	t_l, min	P_B, W	P_P, W	η_S	Ω, rpm	R, m	γ, deg
Maximum loitering time	36.0	160	56	46	0.81	13,600	0.150	0
Minimum noise	18.4	25	357	54	0.15	2230	0.150	0
Minimum noise, $P_B \leq 65$ W	30.7	138	65	43	0.66	7300	0.150	0
Minimum noise, $P_B \leq 70$ W	29.6	129	70	43	0.62	6470	0.150	0
Minimum noise, $P_B \leq 75$ W	28.7	120	75	43	0.58	5900	0.150	0
Minimum noise, $P_B \leq 65$ W, with stress constraints	33.6	138	65	46	0.71	8973	0.137	0
Minimum noise, $P_B \leq 70$ W, with stress constraints	30.6	129	70	44	0.63	6872	0.147	0
Minimum noise, $P_B \leq 75$ W, with stress constraints	29.3	120	75	44	0.59	6086	0.148	0
Minimum noise, $P_B \leq 65$ W, with stress constraints and cone angle	33.3	138	65	46	0.71	8799	0.146	3.3
Minimum noise, $P_B \leq 70$ W, with stress constraints and cone angle	30.5	129	70	44	0.63	6852	0.149	2.2
Minimum noise, $P_B \leq 75$ W, with stress constraints and cone angle	29.0	120	75	44	0.58	6002	0.150	1.4

Table 5 Comparison between the influence of performance constraints, structural constraints, and number of blades for propellers for minimum noise

Design description	N_b	SPLA, min	t_l, min	P_B, W	P_P, W	η_S	Ω, rpm	R, m	γ, deg
Without performance constraints	2	18.4	25	54	357	0.15	2230	0.150	0.0
$P_B \leq 65$ W	2	30.7	138	43	65	0.66	7300	0.150	0.0
$P_B \leq 70$ W	2	29.6	129	43	70	0.62	6470	0.150	0.0
$P_B \leq 75$ W	2	28.7	120	43	75	0.58	5900	0.150	0.0
$P_B \leq 65$ W, with stress constraints and cone angle	2	33.3	138	46	65	0.71	8799	0.146	3.3
$P_B \leq 70$ W, with stress constraints and cone angle	2	30.5	129	44	70	0.63	6852	0.149	2.2
$P_B \leq 75$ W, with stress constraints and cone angle	2	29.0	120	44	75	0.58	6002	0.150	1.4
Without performance constraints	3	−1.7	17	56	535	0.10	1810	0.150	0.0
$P_B \leq 65$ W	3	21.7	138	43	65	0.66	7350	0.150	0.0
$P_B \leq 70$ W	3	19.7	129	43	70	0.62	6500	0.150	0.0
$P_B \leq 75$ W	3	18.1	120	43	75	0.58	5940	0.150	0.0
$P_B \leq 65$ W, with stress constraints and cone angle	3	27.8	138	47	65	0.73	9510	0.140	6.0
$P_B \leq 70$ W, with stress constraints and cone angle	3	21.9	129	45	70	0.64	7070	0.149	2.8
$P_B \leq 75$ W, with stress constraints and cone angle	3	19.5	120	44	75	0.59	6130	0.150	1.2
Without performance constraints	4	−22.1	15	54	608	0.09	1650	0.150	0.0
$P_B \leq 65$ W	4	13.1	138	43	65	0.66	7190	0.150	0.0
$P_B \leq 70$ W	4	9.5	129	43	70	0.62	6480	0.150	0.0
$P_B \leq 75$ W	4	7.3	120	43	75	0.58	5940	0.150	0.0
$P_B \leq 65$ W, with stress constraints and cone angle	4	24.0	138	47	65	0.73	9540	0.111	16.7
$P_B \leq 70$ W, with stress constraints and cone angle	4	13.5	129	45	70	0.65	7210	0.146	3.6
$P_B \leq 75$ W, with stress constraints and cone angle	4	9.7	120	45	75	0.60	6290	0.148	1.4

stress constraints. The increase in the noise is mainly due to the fact that to cope with stress constraints, the rotational speed of the propeller is increased (by 23, 6, and 3% for the cases $P_B \leq 65, 70, 75$ W, respectively), whereas the radius is decreased (by 8.7, 2.0, and 1.3%, respectively). The increase in the rotational speed increases the tensile force along the blade, which results in (due to nonlinear effects) a decrease in the cross-sectional bending moments along the blade (that is caused by the aerodynamic loads). A reduction of the blades' length (reduction of the propeller's radius) also results in a reduction of the cross-sectional bending moment along each blade.

Another method of reducing the bending moment along the blade and thus reducing the stress level is to introduce cone angles at the blades' attachments to the hub. The cone angle is the angle between the blade's axis and the plane of rotation (this plane is perpendicular to the axis of rotation). When there is a positive cone angle, the inertial bending moment (due to the centrifugal forces along the blade) oppose the aerodynamic bending moment (due to the aerodynamic forces). By choosing an appropriate cone angle, the resultant bending moment can be minimized along the blade. In the present case, the cone angle is added as another design variable; thus, the appropriate angle is defined during the optimization process.

The results for the introduction of cone angles are shown at the end of Table 4 for the same three cases: $P_B \leq 65, 70, 75$ W. It is shown that introducing cone angles leads to a small reduction in the noise, due to a small reduction in the rotational speed, compared with the case of stress constraints with zero cone angle. The optimal cone angles are small and decrease with an increase in P_B.

The geometry of the optimal blades for $P_B \leq 70$ W is shown in Fig. 7 for three cases: 1) optimal blade without considering stress constraints (identical results also appear in Fig. 6); 2) optimal blade when stress constraints are included, with zero cone angle; and 3) optimal blade under stress constraints, when the cone angle becomes one of the design variables.

It is clearly shown that adding stress constraints results in a significant increase of thickness along most of the blade. There is also a reduction of the pitch angle at the outer 40% of the blade, which contributes to the reduction of the bending moment at the root region.

D. Influence of the Number of Blades

One of the common methods of reducing propeller noise is to increase the number of blades [5,15,21]. Thus, in addition to the various optimal designs of the previous subsections that dealt with a

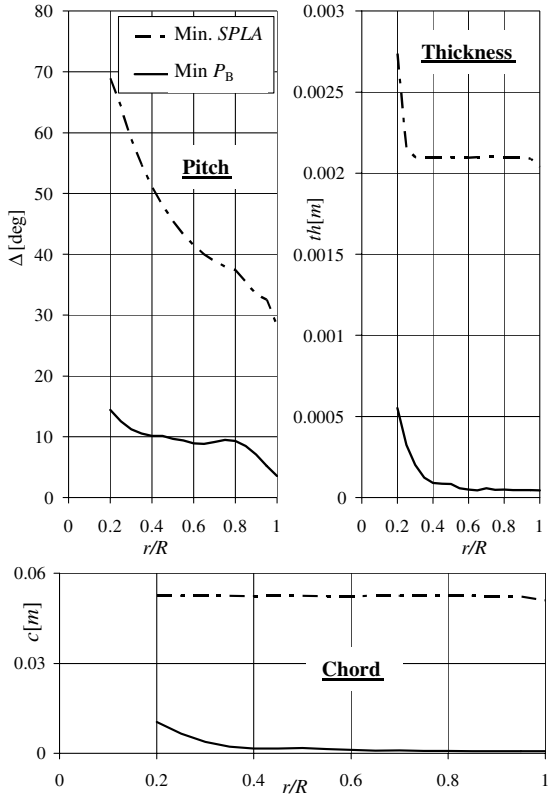

Fig. 5 Geometry of an optimal two-bladed propeller with minimum noise and minimum power propellers.

two-bladed propeller, optimal propellers with three and four blades were also designed. The cost function remains the propeller's SPLA, and the design cases include 1) a quiet propeller without power or structural constraints; 2) a quiet propeller with three kinds of power constraints: $P_B \leq 65, 70, 75$ W, without considering structural constraints; and 3) the same as case 2, but with structural constraints and cone angle as an additional design variable.

Table 5 gives the various optimal designs, and data for a two-bladed propeller from Table 4 is also included for ease of comparisons.

The significant effect of the number of blades on the noise level is clear. The case without any performance or structural constraints

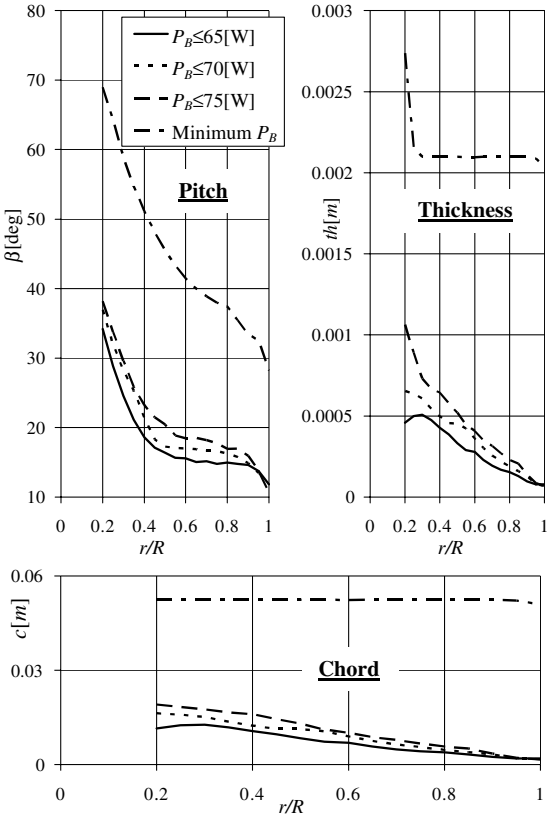

Fig. 6 Geometry of an optimal two-bladed propeller with minimum noise under various power constraints.

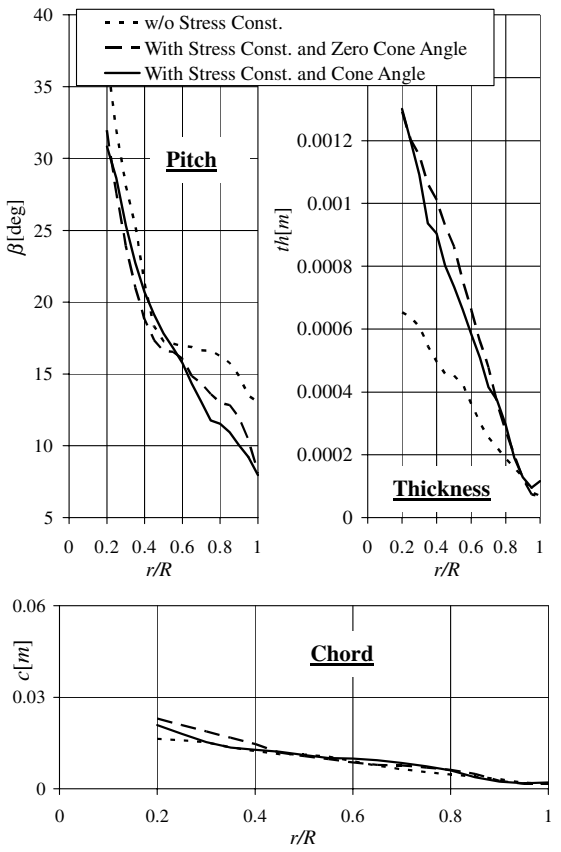

Fig. 7 Influence of structural constraints and cone angle on the minimum noise design with $P_B \leq 70$ W for a two-bladed propeller.

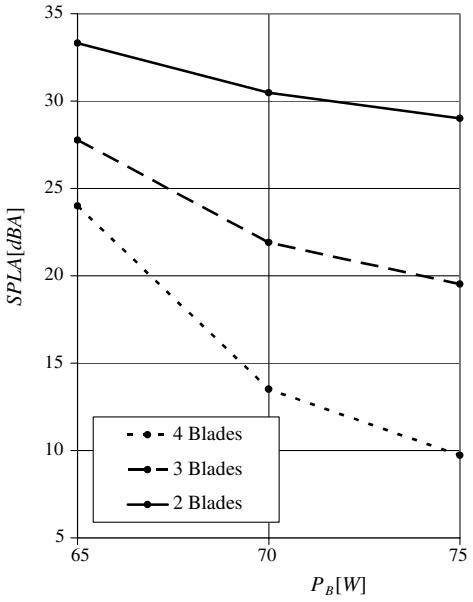

Fig. 8 SPLA of optimal propellers as functions of performance constraints and number of blades for a quiet propeller design with stress constraints.

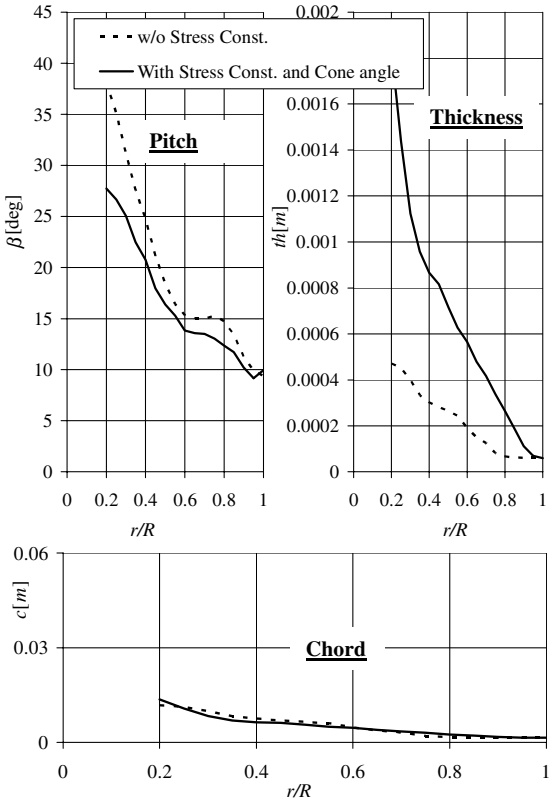

Fig. 9 Influence of structural constraints and cone angle on the minimum noise design with $P_B \leq 70$ W for a four-bladed propeller.

(denoted as "without performance constraints" in Table 5) exhibits a decrease of more than 20 dBA as a result of adding a blade. Unfortunately, loitering time is also reduced significantly, from 25 min (for a two-bladed propeller) to 15 min in the case of four blades. This decrease in loitering time is a result of an increase in the power required by the propeller and decrease in the electric motor efficiency.

When performance constraints are added, the SPLA decrease due to an additional blade becomes 9, 10, and 11 dBA for $P_B \leq 65, 70, 75$ W, respectively. Note that the rotational speed of the optimal propeller depends on the magnitude of the power constraint, but the number of blades has little influence on that speed. In all cases, the optimization leads to the maximum allowable radius of $R = 0.15$ m.

As shown in Table 5, the introduction of stress constraints has a very significant effect on the optimal design for different numbers of blades, in comparison with an optimal design that does not include stress constraints. This effect depends on the magnitude of power constraints.

Figure 8 presents the SPLA of the optimal propellers as functions of the magnitude of the power constraint P_B for various numbers of blades N_b. It is shown that the reduction in SPLA as a result of adding a blade increases with the allowable P_B.

The geometry of a blade of the four-bladed optimal propeller with and without stress constraints for $P_B \leq 70$ W is presented in Fig. 9. This figure is similar to Fig. 7, which presents the same comparison for a two-bladed propeller. The influences of the stress constraints on the optimal design of a quiet propeller were discussed in the previous section. In both cases (two- and four-bladed cases), the influence of the stress constraint on the blade's chord is small, because both blades have to produce the same thrust. The major difference appears in the thickness of the blade, which increases substantially due to the introduction of stress constraints. Whereas the two-bladed case exhibits an increase of about 100%, the four-bladed case increases by more than 200%.

The thicknesses of the optimal two-bladed and four-bladed propellers are similar, but the chord of the four-bladed propeller is smaller than the chord of the two-bladed propeller, and thus the thickness ratio of the four-bladed propeller is higher. This makes the four-bladed propeller less efficient; therefore, an increase in its rotational speed is required. In addition to the increased thickness, to avoid high stresses as the number of blades is increased, the following trends reduce the magnitude of the bending moment along the blade (see Fig. 10):

1) The rotational speed and cone angle are increased.

2) The radius is decreased.

The preceding trends are especially strong in the case in which $P_B \leq 65$ W. Here, the radius is reduced to 0.11 m, and the cone angle becomes 16.7 deg. Such a high cone angle is required to counteract the bending moment due to the aerodynamic forces along the blade.

To understand the very strong influence of the number of blades on the optimal design when $P_B \leq 65$ W, another optimum search was performed. In this case, the optimal propeller for a minimum P_B was designed without imposing any acoustic constraints and with a zero cone angle. The minimal P_B value as a function of the number of blades is presented in Fig. 11. It is shown that for four and five blades, the minimal P_B is larger than 65 W. By introducing cone angles, P_B

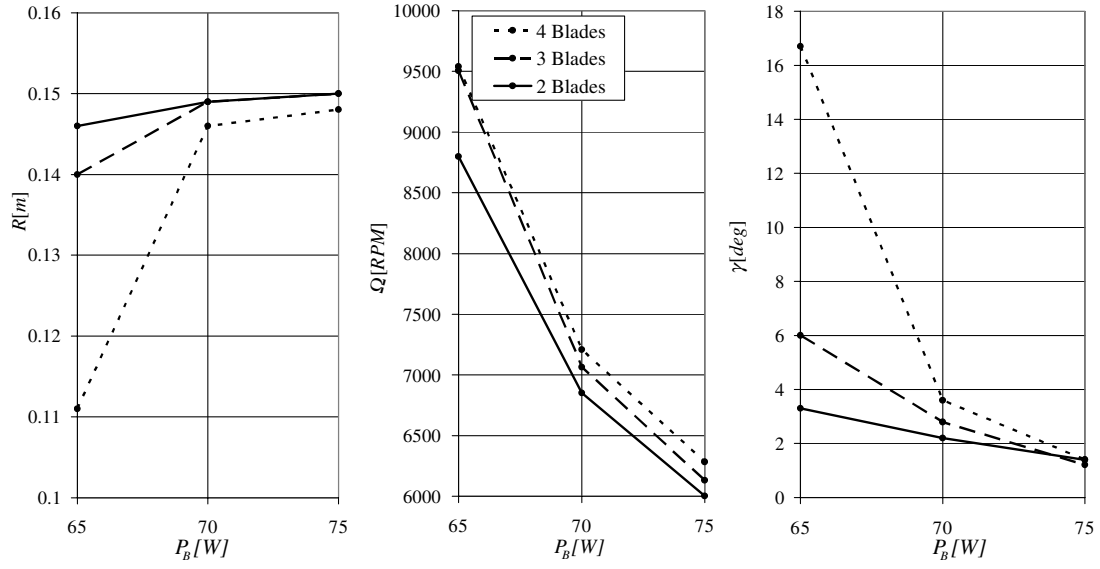

Fig. 10 Radius, rotational speed, and cone angle of the optimal propellers as functions of performance constraint P_B and number of blades N_b for a quiet propeller design under stress constraints.

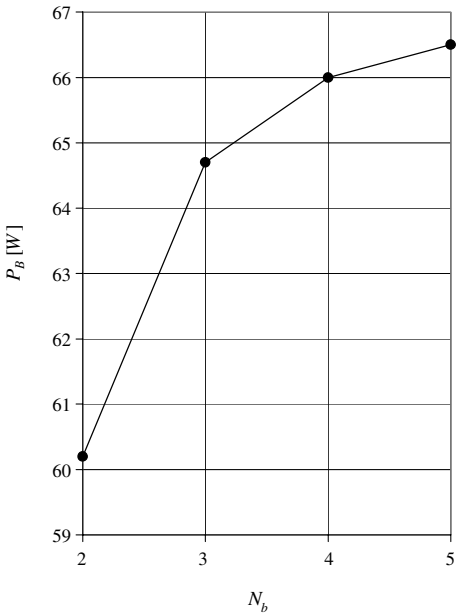

Fig. 11 Minimum P_B as a function of the number of blades under the influence of stress constraints (zero cone angle).

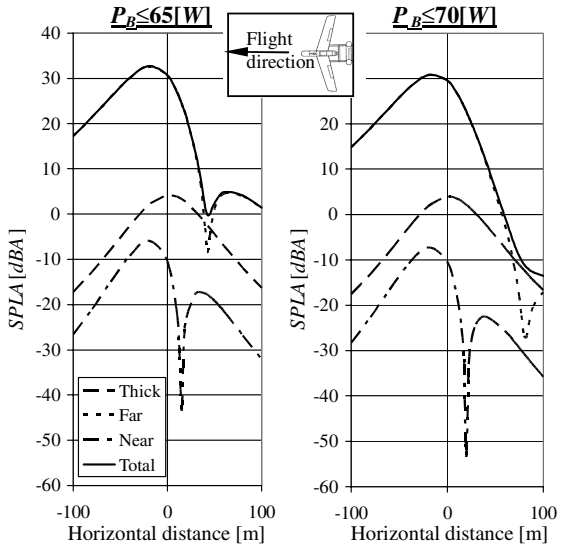

Fig. 13 Noise components of an optimal two-bladed propeller flying at an altitude of 50 m for two different performance constraints (without stress constraints).

can be decreased to 65 W, but this comes at the cost of increasing noise (as shown in Fig. 8).

The optimized blades are very narrow (small chord) at the tip region (see Fig. 7); in some cases, the chord gets below 1 mm. Although these blades withstand structural constraints, such a small chord may not be practical because of manufacturing, maintenance, and reliability aspects. To study this problem and investigate the influence of additional constraints on the optimal design, a side constraint was added that does not allow chord lengths smaller than 6 mm, and few optimizations were run.

In spite of an increase of the chord length in the tip region by almost an order of magnitude, in the cases that were investigated, the relative changes in the propeller parameters, such as required power or rotational speed, were of the order of 10% or less. This may imply that the trends and results that have been presented are also applicable for designs that include additional other constraints (see similar results in [42]).

E. Flyover Noise

The noise in all the previous examples (SPLA) was calculated when the UAV flies 50 m directly above the observer. Yet, in reality, the UAV flies over the observer. Thus, the question arises if optimization for the case in which the UAV is at the zenith point is representative for the entire flyover case. To answer this question, the flyover noise is studied.

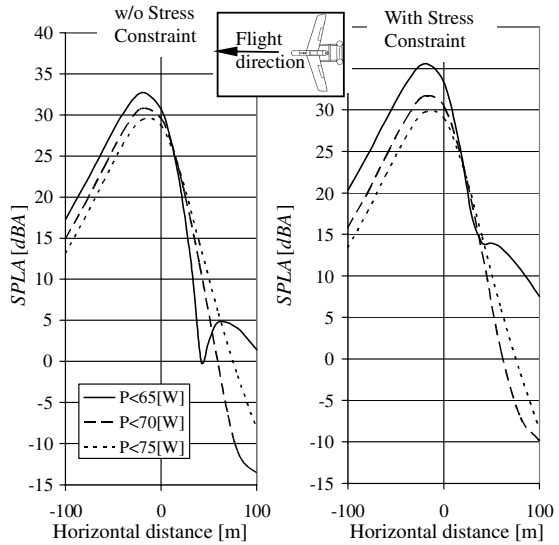

Fig. 12 Influence of different performance constraints on the flyover SPLA of an optimal two-bladed propeller flying at an altitude of 50 m.

Figure 12 presents the SPLA at the observer's point during a flyover of a UAV with a two-bladed propeller. Three optimal propellers are considered, designed under the following three power constraints: $P_B \leq 65, 70, 75$ W. Results for optimizations without and with stress constraints are shown. In each case, the UAV flies at an altitude of 50 m and the SPLA is presented as a function of the horizontal distance (the horizontal projection of the distance between the observer and the vehicle). As shown in the figure, when this distance is positive, the UAV is flying toward the observer, whereas negative distances indicate that it is flying away from the observer.

In both cases, the maximum noise is not obtained when the UAV is at the zenith point, but later, at a horizontal distance of 15–20 m. This distance increases as the constraint becomes stricter (namely, the allowed P_B decreases). For optimal propellers without stress constraints, the maximum SPLA represents an increase of 2.0, 1.3, and 0.9 dBA for $P_B \leq 65, 70, 75$ W, respectively, above the noise at the zenith point. For optimal propellers in the presence of structural constraints, the increase is 2.3, 1.3, and 1.0 dBA for $P_B \leq 65, 70, 75$ W, respectively. In all cases, the trends at the maximum SPLA point are identical to the trends at the zenith point.

Note that whereas the noise is higher for lower values of allowed P_B for the case of a UAV flying away from the observer, the trends may be reversed for an approaching UAV. To further understand the behavior, the various contributions to the resultant noise for a flyover of two optimal propellers ($P_B \leq 65, 70$ W) for an optimal design without stress constraints are presented in Fig. 13. It is shown that the far-field loading noise has the largest contribution and practically determines the resultant SPLA. Although the thickness noise is fairly symmetrical for approaching and receding vehicles, the far-field loading noise decreases with the horizontal distance much faster for an approaching UAV than for a receding one. This unsymmetrical behavior is typical for propeller noise [15,43–45]. The decreasing rate with increasing horizontal distance of the far-field loading noise of the receding UAV changes only slightly as a result of changing the allowable P_B. On the other hand, the rate of decrease with horizontal distance of the far-field loading noise of the approaching vehicle is very sensitive to the allowable P_B, and it increases as the allowable P_B decreases. This is the reason that the trends for an approaching vehicle are reversed compared with a receding UAV. Similar trends have been observed for flyover noise of UAVs with optimal three and four blades.

VI. Conclusions

The paper presents a comprehensive method for the design of quiet propellers that is based on a multidisciplinary design optimization approach. The design of a quiet propeller usually includes a high number of design variables (69–70 design variables in the preceding described examples) and constraints. Thus, to cope with the complexity of this design problem, three different optimization schemes are used that enable the design process to reach a global optimum. The designer is responsible for the definition of the cost function and constraints. In addition, the designer decides on transferring from one optimization scheme to the other.

Often, the design trends of a quiet propeller contradict the design trends of an efficient propeller. Thus, a tradeoff is required to arrive at a practical design. The efficiency of the propulsion system does not depend solely on the propeller, but it is affected significantly by the motor efficiency and the vehicle characteristics. Thus, it is important to include the motor characteristics in the design process.

Based on the design of a quiet propeller for an electric mini UAV, the following conclusions can be drawn:

1) For a given number of blades, the main mechanism of reducing the propeller noise involves a reduction of the propeller's rotational speed.

2) Defining the propeller SPLA as the cost function without applying additional constraints may result in an impractical design of blades with a very large chord and high required power. In the present example, the loitering time for such a design was reduced from 160 min in the case of a maximum loitering time design (without considering any other constraints) to only 25 min for a very quiet propeller deign (without applying any performance constraints).

3) Imposing power constraints (namely, imposing a limit of the extracted power from the battery) increases the propeller noise significantly (compared with a design without such constraints). In the case of a two-bladed propeller, limiting the power to 75 W results in an increase of 10.3 dBA, and a stricter power limit of 65 W results in an increase of 12.3 dBA. This increase in noise is mainly due to the increase in the rotational speed that leads to an improvement in the efficiency of the propulsion system.

4) Imposing stress constraints leads to an increase in the cross-sectional thickness and the rotational speed. Because of the increase in the rotational speed, the SPLA is increased as well (by 1–3 dBA for a two-bladed propeller). It has been shown that by introducing a cone angle, the aerodynamic bending moment is reduced and the optimal propeller's SPLA is decreased by 0.1–0.3 dBA.

5) As the number of blades increases, the noise signature is decreased. The reduction in noise is a function of the power constraint and can reach 10 dBA.

6) The influence of stress constraints on the optimal design depends strongly on the number of blades.

7) During flyover, the noise of a UAV varies as a function of the location of the vehicle relative to the observer. The maximum SPLA is obtained for a receding vehicle shortly after it passes the zenith point. Nevertheless, optimization for a minimum noise at the zenith point reduces the noise signature for most of the flyover case, especially along the noisier parts of the path.

8) For most cases, as the performance constraint becomes more strict (smaller power is allowed), the noise signature increases. Only for an approaching vehicle at certain distances from the observer can this trend be reversed.

9) The far-field loading noise presents the main contribution to the propeller noise. The contributions of the thickness noise and near-field loading noise are usually much smaller.

The results of the present paper emphasize the importance of a multidisciplinary approach during the design of a quiet propeller. It is important to address all the disciplines simultaneously along the design process. Ignoring one of these disciplines may lead to an impractical design.

References

[1] Holmes, J. B., Durham, H. M., and Tarry, E. S., "Small Aircraft Transportation System Concept and Technologies," *Journal of Aircraft*, Vol. 41, No. 1, Jan.–Feb. 2004, pp. 26–35. doi:10.2514/1.3257

[2] Carey, B., "Outlook 2007," *Avionics Magazine* [online journal], Jan. 2007, http://www.aviationtoday.com/av/categories/commercial/7615.html [retrieved 25 Mar. 2007].

[3] Alexander, D., Lee, Y.-M., Guynn, M., and Bushnell, D., "Emissionless Aircraft Study," 38th AIAA/ASME/SAE/ASEE Joint Propulsion Conference and Exhibit, AIAA Paper 2002-4056, July 2002.

[4] Hoehne, V. O., and Luce, R. G., "The Quieted Aircraft as a Military Tool," AIAA Paper 1969-792, 1969.

[5] Cross, J. L. and Watts, M. E., "In Flight Acoustic Testing Techniques Using the YO-3A Acoustic Research Aircraft," 2nd AIAA/AHS/IES/SETP/SFTE/DGLR Flight Testing Conference, Las Vegas, NV, AIAA Paper 83-2754, Nov. 1983.

[6] Fulghum, A. D., "Stealth Now," *Aviation Week and Space Technology*, Vol. 162, No. 13, May 2005, p. 38.

[7] Keennon, M. T., and Grasmeyer, J. M., "Development of the Black Widow and Microbat MAVs and a Vision of the Future of MAV Design," AIAA/ICAS International Air and Space Symposium and Exposition: The Next 100 Years, Dayton, OH, AIAA Paper 2003-2901, July 2003.

[8] Lawrence, D. A., and Mohseni, K., "Efficiency Analysis for Long-Duration Electric MAVs," AIAA Infotech@Aerospace, Arlington, VA, AIAA Paper 2005-7090, Sept. 2005.

[9] Nagel, A., Levy, D. E., and Shepshelovich, M., "Conceptual Aerodynamic Evolution of Mini/Micro UAV," 44th AIAA Aerospace Sciences Meeting and Exhibit, Reno, NV, AIAA Paper 2006-1261, Jan. 2006.

[10] Logan, M. J., Chu, J., Motter, M. A., Carter, D. L., Ol, M., and Zeune, C., "Small UAV Research and Evolution in Long Endurance Electric Powered Vehicles," AIAA Infotech@Aerospace, AIAA Paper 2007-2730, May 2007.

[11] Sobieszczanski-Sobieski, J., and Haftka, R. T., "Multidisciplinary Aerospace Design Optimization: Survey of Recent Developments," *Structural Optimization*, Vol. 14, 1997, pp. 1–23. doi:10.1007/BF01197554

[12] Betz, A., *Schraubenpropeller mit Geringstem Energieverlust*, Vol. 2, Königliche Gesellschaft der Wissenschaften, Göttingen, Germany, 1919, pp. 193–217; also *Screw Propeller with Minimum Energy Loss*, Technical Translation 736, translated by D. A. Sinclair, National Research Council Library, Ottawa, 1958.

[13] Adkins, C. N., and Liebeck, R. H., "Design of Optimum Propellers," *Journal of Propulsion and Power*, Vol. 10, No. 5, Sept.–Oct., 1994, pp. 676–682. doi:10.2514/3.23779

[14] Roncz, G. J., "Propeller Development for the Rutan Voyager," General Aviation Aircraft Meeting and Exposition, Wichita, KS, Society of Automotive Engineers Paper SAE-891034, Apr. 1989.

[15] Succi, G. P., "Design of Quiet Efficient Propellers," SAE Business Aircraft Meeting, Society of Automotive Engineers Paper SAE79-0584, Apr. 1979.

[16] Patrick, H., Finn, W. R., and Stich, K. C., "Two and Three-Bladed Propeller Design for the Reduction of Radiated Noise," 3rd AIAA/CEAS Aeroacoustics Conference, Atlanta, GA, AIAA Paper 97-1710-CP, May 1997.

[17] Ormsbee, A. I., and Woan, C. J., "Optimum Acoustic Design of Free Running Low Speeds Propellers," AIAA Aircraft Systems and Technology Meeting, Seattle, WA, AIAA Paper 77-1248, Aug. 1977.

[18] Miller, J. C., and Sullivan, P. J., "Noise Constraints Effecting Optimal Propeller Designs," SAE General Aviation Aircraft Meeting and Exposition, Wichita, KS, Society of Automotive Engineers Paper 85-0871, Apr. 1985.

[19] Burger, C., Hartfield, J. R., and Burkalter, J., "Performance and Noise Optimization of a Propeller Using the Vortex Lattice Method and a Genetic Algorithm," 48th AIAA/ASME/ASCE/AHS/ASC Structures, Structural Dynamics, and Materials Conference, Honolulu, HI, AIAA Paper 2007-1883, Apr. 2007.

[20] Patrick, H., Finn, R. W., and Stich, C. K., "Two- and Three-Bladed Propeller Design for the Reduction of Radiated Noise," 3rd AIAA/CEAS Aeroacoustics Conference, Atlanta, GA, AIAA Paper 97-1710, 12–14 May, 1997.

[21] Drack, E. L., and Wood, A. L., "DESIGN AND Analysis of Propellers for General Aviation Aircraft Noise Reduction," 21st ICAS Congress, Melbourne, Australia, International Council of Aeronautical Sciences Paper 98-5.11.3, Sept. 1998.

[22] Janus, J. M., "General Aviation Propeller-Airframe Integration Simulation," *Journal of Aircraft*, Vol. 43, No. 2, Mar.–Apr. 2006, pp. 390–394. doi:10.2514/1.15354

[23] Gur, O., and Rosen, A., "Comparison Between Blade-Element Models of Propellers," *The Aeronautical Journal*, Vol. 112, No. 1138, Dec. 2008, pp. 689–704.
[24] Gur, O., and Rosen, A., "Propeller Performance at Low Advance Ratio," *Journal of Aircraft*, Vol. 42, No. 2, Mar.–Apr. 2005, pp. 435–441.
doi:10.2514/1.6564
[25] Yamamoto, O., and Aug., R., "Structural and Aerodynamic Analysis of a Large-Scale Advanced Propeller Blade," *Journal of Propulsion and Power*, Vol. 8, No. 2, Mar.–Apr., 1992, pp. 367–373.
doi:10.2514/3.23487
[26] Rosen, A., and Gur, O., "A Transfer Matrix Model of Large Deformations of Curved Rods," *Computers and Structures*, E-first publication Feb. 2009.
doi:10.1016/j.compstruc.2008.12.014
[27] Ffowcs, J. E. W., and Hawkings, D. L., "Sound Generation by Turbulence and Surfaces in Arbitrary Motion," *Philosophical Transactions of the Royal Society of London, Series A: Mathematical and Physical Sciences*, Vol. 264, 1969, pp. 321–342.
doi:10.1098/rsta.1969.0031
[28] Magliozzi, B., Hanson, D. B., and Amiet, K. R., "Aeroacoustics of Flight Vehicles Theory and Practice," edited by H. H. Hubbard, NASA TR 90-3052, Aug. 1991.
[29] Hanson, D. B., and Fink, M. R., "The Importance of Quadrupole Sources in Prediction of Transonic Tip Speed Propeller Noise," *Journal of Sound and Vibration*, Vol. 61, No. 1, 1978, pp. 19–38.
[30] Farassat, F., and Succi, G. P., "A Review of Propeller Discrete Frequency Noise Prediction Technology with Emphasis on Two Current Methods for Time Domain Calculations," *Journal of Sound and Vibration*, Vol. 71, No. 3, 1980, pp. 399–419.
doi:10.1016/0022-460X(80)90422-8
[31] Sanford, F., Pearsons, K. S., and Bennett, R. L., "Predicting Aural Detectability of Aircraft in Noise Background," U.S. Air Force Flight Dynamics Lab. TR 72-17, Wright–Patterson AFB, OH, July 1972.
[32] Dobrzynski, W. M., Heller, H. H., Powers, J. O., and Densmore, J. E., "DFVLR/FAA Propeller Noise Test in the German-Dutch Wind Tunnel DNW," Federal Aviation Administration Rept. AEE 86-3, 1986.
[33] Magliozzi, B., "The Influence of Forward Flight on Propeller Noise," NASA CR 145105, 1977.
[34] Succi, G. P., "Computed and Experimental Spectra for a Wing Mounted Microphone on a Light STOL Aircraft," NASA CR 165725, May 1978.
[35] Borst, V. H., "Summary of Propeller Design Procedures and Data," Vol. 1, U.S. Army Air Mobility Research and Development Lab., TR 73-34A-VOL-1, Nov. 1973.
[36] Boyd, S., and Vandenberghe, L., *Convex Optimization*, Cambridge Univ. Press, New York, 2004, p. 716.
[37] Goldberg, E. D., *Genetic Algorithms in Search, Optimization, and Machine Learning*, Addison Wesley, Reading, MA, 1989, p. 412.
[38] Nelder, J. A., and Mead, R., "A Simplex Method for Function Minimization," *Computer Journal*, Vol. 7, No. 4, 1965, pp. 308–313.
[39] Van der Velden A., "Tools for Applied Engineering Optimization," AGARD Rept. R-803, Neuilly-sur-Seine, France, Apr. 1994
[40] Gur, O., and Rosen, A., "Optimization of a Propeller Based Propulsion System ," *Journal of Aircraft*, Vol. 46, No. 1, Jan.–Feb. 2000, pp. 95–106.
[41] Sullivan, J. P., Chang, L. K., and Miller, C. J., "The Effect of Proplets and Bi-Blades on the Performance and Noise of Propellers," SAE Business Aircraft Meeting and Exposition, Wichita, KS, Society of Automotive Engineers Paper 810600, Apr. 1981.
[42] Gur, O., and Rosen, A., "Optimizing Electric Propulsion Systems for UAV's," 12th AIAA/ISSMO Multidisciplinary Analysis and Optimization Conference, Victoria, BC, Canada, AIAA Paper 2008-5916, Sept. 2008.
[43] Hanson, D. B., "The Influence of Propeller Design Parameters on Far Field Harmonics Noise in Forward Flight," AIAA 5th Aeroacoustics Conference, Seattle, WA, AIAA Paper 79-0609, Mar. 1979.
[44] Herkes, W., "An Experimental Study of the Noise Generated by a Pusher Propeller Due to Wake Entering the Propeller Disc," von Karman Inst. for Fluid Dynamics, Rept. 1979-17, Rhode-St-Genèse, Belgium, Nov., 1979.
[45] Heller, H., "Propeller Aircraft Noise-Certification and Flight-Testing," Deutsche Forschungs- und Versuchsanstalt für Luft- und Raumfahrt, Paper 82-16, Oct. 1982.

C. Tan
Associate Editor